Disruption of riboflavin biosynthesis in mycobacteria establishes 5-amino-6-D-ribitylaminouracil (5-A-RU) as key precursor of MAIT cell agonists

Melissa D. Chengalroyen[1¶], Nurudeen Oketade[2¶], Aneta Worley[3], Megan Lucas[2], Luisa Nieto Ramirez[2], Mabule L. Raphela[1], Gwendolyn M. Swarbrick[3], Digby F. Warner[1,4], Deborah A. Lewinsohn[3], Carolina Mehaffy[2], Erin J. Adams[5], William Hildebrand[6], Karen M. Dobos[2*], Valerie Mizrahi[1,4*] and David M. Lewinsohn[3,7*]

[1]UCT Molecular Mycobacteriology Research, Institute of Infectious Disease and Molecular Medicine, Department of Pathology, University of Cape Town, Cape Town, South Africa

[2]Department of Microbiology, Immunology and Pathology, Colorado State University, Colorado, United States of America

[3]Oregon Health and Science University, Oregon, United States of America

[4]Wellcome Centre for Infectious Disease Research in Africa, University of Cape Town, South Africa

[5]Department of Biochemistry and Molecular Biology, University of Chicago, Chicago, Illinois, United States of America

[6]Department of Microbiology and Immunology, University of Oklahoma Health Sciences Centre, Oklahoma City, Oklahoma, United States of America

[7]Portland VA Medical Center, Oregon, United States of America

* Corresponding authors

Email: karen.dobos@colostate.edu (KD); valerie.mizrahi@uct.ac.za (VM); lewinsod@ohsu.edu (DML)

¶These authors contributed equally to this work.

Abstract

Mucosal-associated invariant T (MAIT) cells exhibit an intrinsic ability to recognize and respond to microbial infections. The semi-invariant antigen recognition receptor of MAIT cells specifically detects the non-polymorphic antigen-presenting molecule, major histocompatibility complex class I-related protein 1 (MR1), which primarily binds riboflavin-derived metabolites of microbial origin. To further interrogate the dependence of these antigens on riboflavin biosynthesis in mycobacteria, we deleted individual genes in the riboflavin biosynthesis pathways in *Mycobacterium smegmatis* (Msm) and *Mycobacterium tuberculosis* (Mtb) and evaluated the impact thereof on MAIT cell activation. Blocking the early steps of the pathway by deletion of RibA2 or RibG profoundly reduced, but did not completely ablate, MAIT cell activation by Msm or Mtb, whereas deletion of RibC, which catalyzes the last step in the pathway, had no significant effect. Interestingly, deletion of RibH specifically enhanced MAIT cell recognition of Mtb whereas loss of lumazine synthase (RibH) activity had no impact on MAIT cell activation by Msm. MAIT cell activation by Msm was likewise unaffected by blocking the production of the MAIT cell antagonist, F_o (by inhibiting its conversion from the riboflavin pathway intermediate, 5-amino-6-D-ribitylaminouracil (5-A-RU), through the deletion of *fbiC*). Together, these results confirm a central role for 5-AR-U in generating mycobacterial MR1 ligands and reveal similarities and differences between Msm and Mtb in terms of the impact of riboflavin pathway disruption on MAIT cell activation.

Author summary

Mucosal-associated invariant T (MAIT) cells are an abundant population of innate-like T-cells which respond to microbial infections. These specialized cells recognize the MR1 molecule, which presents microbial metabolites derived from riboflavin (vitamin B2) biosynthesis. These

53 cells are enriched in the airways, and, in some cases, reduced in the peripheral blood of
54 tuberculosis (TB) infected individuals suggestive of a role in the early response to infection by
55 *Mycobacterium tuberculosis*. In this study, we investigated the effect of deleting individual
56 genes in the riboflavin biosynthesis pathway on MAIT cell activation by *Mycobacterium*
57 *tuberculosis* or *Mycobacterium smegmatis*. Our findings revealed that disrupting early stages
58 in the pathway profoundly reduced, but did not eliminate MAIT cell activation by both
59 mycobacterial species. However, blocking the penultimate step in the pathway, catalyzed by
60 the enzyme, lumazine synthase, led specifically to increased MAIT cell recognition of *M.*
61 *tuberculosis*. Our results confirm the pivotal role of the riboflavin pathway intermediate, 5-A-
62 RU, in generating mycobacterial ligands that serve as MAIT cell agonists. By enhancing our
63 understanding of how MAIT cells recognize mycobacterial infections, the results of this study
64 could inform strategies for the development of vaccines and/or immunotherapies for TB.
65

66 # Introduction

67 MR1-restricted T cells (MR1Ts) are characterized by their dependence on the highly conserved
68 molecule, MR1 [1]. A subset of MR1Ts, Mucosal Associated Invariant T cells (MAITs), have
69 been characterized by their usage of a semi-invariant T cell receptor (TRAV1-2) [1, 2], their
70 expression of the transcription factor PLZF, and expression of CD161 and CD26 [3]. While
71 these cells are among the most abundant in the human circulation and in mucosal sites, their
72 function was largely unknown until 2010 when they were found to recognize a variety of
73 microbes including the major human pathogen, *Mycobacterium tuberculosis* (Mtb) [4, 5]. A
74 seminal discovery was made in 2012 when Kjer-Nielsen *et al*. [6] demonstrated that MR1 could
75 present the metabolite, 5-(2-oxopropylideneamino)-6-D-ribitylaminouracil (5-OP-RU),
76 derived from an intermediate in the riboflavin biosynthesis pathway of *Salmonella* sp., to
77 MAIT cells. These authors argued that microbes producing riboflavin are uniquely poised to

78 activate these cells. Microbially derived MR1 ligands and antigens have since been found to
79 be more diverse than originally described [7]; others that have been discovered include
80 photolumazines I, III and V, which were identified in *Mycobacterium smegmatis* (Msm) and
81 are also derived from the riboflavin pathway [8, 9]. However, the source of MR1 ligands that
82 are stimulatory for MAIT cells may extend beyond the riboflavin pathway as evidenced by our
83 finding that the TRAV1-2-negative, TRAV12-2-expressing T-cell clone, D462-E4, recognizes
84 ligands derived from *Streptococcus pyogenes*, a riboflavin auxotroph [10]. This suggests that
85 MR1Ts can distinguish between microbes in a TCR-dependent manner.

86 The central role of the microbial riboflavin pathway in MAIT cell activation has been
87 confirmed in different organisms. These include deletion mutants of *Lactococcus lactis* [7],
88 *Salmonella* Typhimurium [11], *Escherichia coli* [12], *Streptococcus pneumoniae* [13] and
89 *Aspergillus fumigatus* [14] rendered auxotrophic for riboflavin as well as natural variants of *S.*
90 Typhimurium [15] and *S. pneumoniae* [13] with altered expression of the riboflavin pathway.
91 Moreover, engineered overexpression of specific riboflavin pathway genes in Msm, Mtb or *M.*
92 *bovis* BCG was shown to enhance MAIT cell activation, albeit differentially between the three
93 mycobacterial species and to varying extents, depending on the gene targeted for over-
94 expression [16]. Building on our prior work demonstrating the essentiality of riboflavin
95 biosynthesis in Mtb and Msm, and the ability of both organisms to transport and assimilate
96 riboflavin [17], we set out to investigate the impact of riboflavin pathway disruption on MAIT
97 cell activation by these mycobacteria. We generated mutants of Mtb and Msm auxotrophic for
98 this cofactor by knocking out individual genes in the biosynthesis pathway and analyzed the
99 impact thereof on the expression of the pathway genes and proteins, and on MAIT cell
100 activation. We show that blocking the early steps of the pathway by deleting either RibA2 or
101 RibG profoundly reduced but did not completely eliminate MAIT cell activation whereas
102 deletion of RibC, which catalyzes the last step in the pathway, had no discernable effect on

103 MAIT cell activation by Msm or Mtb. Moreover, deletion of RibH specifically enhanced MAIT
104 cell recognition of Mtb whereas loss of lumazine synthase activity had no significant impact
105 on MAIT cell activation by Msm. MAIT cell activation by Msm was likewise unaffected by
106 blocking the production of the MAIT cell antagonist, F_0, which is derived from the riboflavin
107 pathway intermediate, 5-A-RU, by deletion of *fbiC*. Our results confirm a central role for 5-A-
108 RU in the production of mycobacterial MR1 ligands and reveal similarities and differences
109 between Msm and Mtb in terms of the impact of riboflavin pathway disruption on MAIT cell
110 activation. These findings will guide future studies in the field of MR-1 immune responses
111 towards Mtb.

112 Results

113 Construction of deletion mutants in the riboflavin pathway of
114 Msm and Mtb

115 In a recent study [17], we characterized the riboflavin biosynthesis pathway in Mtb H37Rv and
116 Msm mc^2155 and confirmed that it comprises a bifunctional GTP cyclohydrolase II/3,4-DHBP
117 synthase (RibA2); riboflavin deaminase/5-amino-6-(5-phosphoribosylamino) uracil reductase
118 (RibG); an unidentified phosphatase; lumazine synthase (RibH), and riboflavin synthase
119 (RibC) (**Fig 1A and 1B**). Riboflavin is the precursor of flavin mononucleotide (FMN) and
120 flavin adenine dinucleotide (FAD), which are produced by the bifunctional enzyme, RibF. The
121 biosynthetic pathway also leads to the production of the deazaflavins, F_0 and F_{420}, from the
122 pathway intermediate, 5-A-RU, via the sequential action of the enzymes FbiC, FbiA and FbiB
123 [18]. Together, the flavin and deazaflavin cofactors enable the activity of a myriad enzymes in
124 mycobacteria, organisms which adopt 'flavin-intensive' lifestyles [19, 20].
125

126 **Fig 1. Riboflavin biosynthesis and utilization pathways in mycobacteria. (A)** In the
127 biosynthesis pathway, ribulose-5-P and GTP are converted to 3,4-dihydroxyl-2-butanone 4-
128 phosphate (3,4-DHBP) and 2,5-diamino-6-(5-phospho-D-ribosylamino)-pyrimidin-4(3H)-one
129 (DARPP), respectively, by the bifunctional GTP cyclohydrolase II/ DHBP synthase, RibA2.
130 DARPP is deaminated and the side chain subsequently reduced by the bifunctional riboflavin
131 deaminase/ 5-amino-6-(5-phosphoribosylamino) uracil reductase, RibG, to form 5-amino-6-
132 ribitylamino-2,4(1H,3H)-pyrimidinedione-5-phosphate (ArPP). Dephosphorylation of ArPP
133 by an unknown phosphatase generates 5-amino-6-D-ribitylaminouracil (5-A-RU). 5-A-RU
134 together with 3,4-DHBP are condensed by the lumazine synthase, RibH (RibH1/RibH2), to
135 yield 6,7-dimethyl-8-ribityllumazine (DMRL). Two molecules of DMRL are converted to
136 riboflavin and 5-A-RU by the riboflavin synthase, RibC via a dismutation reaction. In the
137 utilization pathway, riboflavin is converted to FMN and FAD by the bifunctional kinase/ FAD
138 synthetase, RibF. The deazaflavin, F_{420}, is produced from 5-A-RU by the sequential action of
139 FbiC, FbiA and FbiB. The deletion mutations are shown in red. (**B)** Genomic context of the
140 riboflavin biosynthesis genes in Msm and Mtb.
141
142 A notable difference between Msm and Mtb is the redundancy in lumazine synthase
143 activity in Msm where this function is served by a canonical RibH (MSMEG_3073, designated
144 herein as RibH1) – the homologue of the sole RibH in Mtb (Rv1416) – and a second
145 homologue, MSMEG_6598, designated here as RibH2 [17]. In prior work, we used a panel of
146 inducible CRISPRi hypomorphs in genes involved in riboflavin biosynthesis and utilization to
147 confirm the essentiality of the riboflavin pathway for mycobacterial growth and survival *in*
148 *vitro* and demonstrate that Mtb and Msm can transport and assimilate exogenous riboflavin
149 [17]. However, residual expression of target genes in induced hypomorphs could confound the
150 ability to differentiate the contributions of individual riboflavin pathway intermediates in

151 MAIT cell recognition of mycobacteria. To avoid this potential complication, we created a
152 Msm and Mtb riboflavin auxotrophs carrying deletions in individual genes in the riboflavin
153 biosynthesis pathway for the purpose of this study (**S1 Fig**). Importantly, the deletion mutations
154 in *ribA2* eliminated both GTP cyclohydrolase II and DHBP synthase domains of RibA2, which
155 catalyze the first and penultimate steps in the pathway, respectively.

156 The growth phenotypes of the Msm and Mtb mutants and their complemented
157 counterparts were assessed in liquid and on solid media, with or without riboflavin supplement
158 **(Fig 2 and S2 Fig)**. The Msm Δ*ribA2*, Δ*ribG*, Δ*ribH2*Δ*ribH1* and Δ*ribC* mutants, and the Mtb
159 Δ*ribA2*, Δ*ribH* and Δ*ribC* mutants were auxotrophic for riboflavin whereas the Msm Δ*fbiC*
160 mutant showed no growth phenotype. Limited complementation of the growth kinetics in liquid
161 culture was observed for the Msm Δ*ribA2*, Δ*ribH1* and Δ*ribH2*Δ*ribH1* strains (complemented
162 with *ribH2* or both) whereas restoration of growth approximating the corresponding wildtype
163 was observed for the other complemented strains. The riboflavin auxotrophy of the Mtb Δ*ribH*
164 and Msm Δ*ribH2*Δ*ribH1* mutants confirmed that under the conditions tested, these organisms
165 depend on the enzymatic production of DMRL by lumazine synthase and as such, this cellular
166 function cannot be served by non-enzymatic production of this pathway intermediate [21].
167

168 **Fig 2. Growth kinetics of wildtype, knockout and complemented mutant strains of Msm**
169 **(A) and Mtb (B) in 7H9 media.** Error bars represent standard deviation from two biological
170 replicates. Statistical comparisons, against wildtype were performed using a one-way ANOVA
171 and Dunnett's multiple comparison test whereby statistical significance is represented by $p <$
172 0.005, shown by an asterisk.
173

174 Riboflavin pathway transcript and protein levels in the Msm wildtype, knockout and
175 complemented strains were measured by qRT-PCR and Data Independent Acquisition (DIA)

176 proteomics, respectively (**Fig 3**). As the auxotrophs required riboflavin for growth, we assessed
177 the impact of riboflavin supplement on the levels of riboflavin pathway transcripts and proteins
178 in wildtype Msm and found no significant effects. The absence of the cognate transcript and
179 protein was confirmed in the knockout mutants with variable restoration thereof in the
180 complemented derivatives in a manner consistent with the corresponding growth phenotypes
181 (**Fig 2 and S2**). Certain knockouts also affected the expression of other members of the
182 pathway, e.g., a 3-fold increase in *ribH2* transcript and RibH2 protein was observed in the Msm
183 Δ*ribH1* mutant suggesting a regulatory interdependence of expression between the two
184 lumazine synthases **(Fig 3G and H).** However, the Δ*ribH1* mutant was still growth impaired
185 relative to wildtype **(Fig 2)** indicating that RibH2 cannot fully compensate for the loss of RibH1
186 in Msm, which suggests that RibH1 is the main catalytic enzyme for production of riboflavin.
187 We observed some differences in the effect of pathway gene knockout *vs*. knockdown on
188 expression of other genes in the pathway, *e.g*., silencing of *ribH1* led to an upregulation of *ribG*
189 and *ribF*, and silencing of *ribA2* suppressed the expression of *ribG*, *ribC* and *ribH1* in Msm
190 [17] but such effects were not observed by knockout of *ribH1* or *ribA2.* The differences may
191 be due in part to the fact that the target proteins were only partially depleted in the knockdowns
192 under the conditions of the expression analysis [17] but are entirely absent in the knockouts.
193
194 **Fig 3. Quantification of riboflavin pathway transcript protein levels in Msm strains. (A,**
195 **C, E, G and I)** Fold change in *sigA*-normalized transcript levels relative to wildtype. **(B, D, F,**
196 **H and J)** Protein abundance was measured using DIA. Data are shown as mean quantification
197 ± SEM from two biological replicates. Statistical comparisons were performed using a one-
198 way ANOVA and Sidak's multiple comparison test whereby statistical significance is
199 represented by $p<0.05$, $p<0.001$, $p<0.0005$ $p<0.0001$, shown by *, **, ***, **** respectively.

200 The Mtb Δ*ribA2*, Δ*ribH* and Δ*ribC* mutants likewise showed riboflavin auxotrophy
201 with riboflavin-independent growth restored by genetic complementation. Knockout and
202 complementation of *ribA2, ribH* and *ribC* were further validated by transcript and protein
203 quantification (**Fig 4**). Additionally, stable isotope-labeled standards were made for peptides
204 derived from RibA2, RibC and RibH with the goal of determining absolute peptide
205 concentration and, by inference, the concentration of the intact protein using parallel reaction
206 monitoring (PRM) (**S3 Fig**). Riboflavin supplement suppressed expression of *ribC* and
207 enhanced expression of *ribA2* in wildtype Mtb **(Fig 4A and E)** but had no significant impact
208 on expression of other pathway genes. Knockout of other pathway genes had no effect on
209 RibA2 abundance but there was a reduction in expression of *ribA2* in the Δ*ribC* mutant which
210 was restored by complementation **(Fig 4A and B)**. RibH transcript and protein levels were
211 markedly lower than wildtype in the complemented Mtb Δ*ribH* strain **(Fig 4C and D)** but still
212 sufficient to restore growth to wildtype levels **(Fig 2)**. In contrast, *ribH* transcript and RibH
213 protein levels were increased 12-to-16-fold in the Δ*ribA2* mutant and its complement vs.
214 wildtype **(Fig 4C and D)**, a finding confirmed by absolute quantification of RibH using PRM
215 and likely due to the presence of a vector-borne promoter/s upstream of *ribH* in the Δ*ribA2*
216 mutant (**S1 Fig**).
217
218 **Fig 4. Quantification of riboflavin pathway transcript protein levels in Mtb strains. (A,**
219 **C, and E)** Fold change in *sigA*-normalized transcript levels relative to wildtype. Data are
220 shown as mean quantification ± SEM from three biological replicates. **(B, D, and F)** Protein
221 abundance was measured using DIA. Statistical comparisons were performed using a one-way
222 ANOVA and Sidak's multiple comparison test whereby statistical significance is represented
223 by $p<0.05$, $p<0.001$, $p<0.0005$, $p<0.0001$, shown by *, **, ***, **** respectively. ns, not
224 significant.

225

226 Deletion of *ribA2* or *ribG* selectively ablates MAIT cell activation 227 by Msm

228 To assess the impact of disrupting the riboflavin biosynthesis pathway on MAIT cell activation,
229 Msm cultures grown in the presence of riboflavin were used to assess the ability to activate a
230 panel of four MR1 restricted T cell clones: D426-G11, D481-C7 and D481-F12, TRAV1-2+
231 MAIT cell clones with varied TCRα chains **(S1 Table)** [8], and D520-E10, a TRAV1-2- MR1T
232 clone [8]. These were selected to reflect the diversity of ligands seen by MR1Ts with D481 C7
233 uniquely able to detect the photolumazine antigens derived from Msm [8]. Each clone was
234 tested by IFN-γ ELISPOT for its ability to recognize dendritic cells infected with mycobacteria
235 at an MOI of 10 (**Fig 5**). Deletion of *ribA2* or *ribG* resulted in an 82-99% reduction in T cell
236 recognition of Msm for all clones tested, a phenotype reversed by complementation. In
237 contrast, deletion of *ribC* had no significant impact on T cell activation by Msm (**Fig 5**).
238 Deletion of *ribH1* and *ribH2* alone or in combination had no impact on recognition of Msm by
239 the three TRAV1-2+ clones, D426-G11, D481-C7 and D481-F12, whereas recognition of the
240 TRAV1-2- clone, D520-E10, was reduced compared to wildtype response. However, this effect
241 was not reversed by complementation, presumably due to the lack of complementation of
242 *ribH1* deficiency revealed by growth phenotyping and expression analyses of the Δ*ribH1* and
243 Δ*ribH2*Δ*ribH1* mutants (**Fig 2 and Fig 3**). Nonetheless, the diminished response of this clone,
244 which uniquely recognizes Msm, implies that the antigen recognized by this clone could be a
245 lumazine.

246 In addition to its role as a substrate of RibH and precursor of DMRL, 5-AR-U is also
247 required for the production of the deazaflavin MAIT cell antagonist, F_0 [18], via the action of
248 FbiC. We therefore assessed the effect of blocking this route of 5-A-RU metabolism on MAIT

249 cell activation using a *fbiC* deletion mutant of Msm. The Δ*fbiC* mutation had no effect on Msm
250 viability (**Fig 2**) or recognition by the TRAV1-2+ T cell clones, D426-G11 and D481-C7 (**Fig**
251 **5**). However, there was a trend towards reduced recognition of Msm by the TRAV1-2+ clone,
252 D481-F12, and the TRAV19-1 clone, D510-E10 (**Fig 5**). This again might suggest preferential
253 recognition of the lumazine antigens found in Msm.
254
255 **Fig 5. Impact of riboflavin pathway mutations on MR1T recognition of Msm**. MR1T cell
256 clone (1e4) IFN-γ response to DCs (1e4) incubated with Msm at a MOI of 10. Response was
257 normalized to wildtype Msm. Data are representative of n=3 independent experiments.
258 Statistical comparisons were performed using a one-way ANOVA and Sidak's multiple
259 comparison test whereby statistical significance is represented by $p<0.05$, $p<0.001$, $p<0.0005$
260 $p<0.0001$, shown by *, **, ***, **** respectively.
261

262 Opposite effects of *ribA2* vs. *ribH* deletion on MAIT cell activation
263 by Mtb

264 The Mtb strains were tested for their ability to activate three of the MR1 restricted T cell clones
265 described above, namely, D426-G11, D481-C7, and D481-F12 (**Fig 6**). The TRAV1-2- clone
266 D520-E10 was not used in this experiment as it is unable to recognize Mtb **(S4 Fig)**. Each clone
267 was tested by IFN-γ ELISPOT for its ability to recognize the BEAS-2B bronchial epithelial
268 cell line infected with Mtb at an MOI of 10. As the strains varied in their ability to activate the
269 MAIT cell clones, we normalized these responses to the HLA-B45, Mtb8.4-specific clone [22].
270 As observed in Msm, the deletion of *ribA2* in Mtb reduced T cell recognition of all clones by
271 87-97%, an effect restored by complementation. On the other hand, the deletion of *ribH*
272 significantly enhanced recognition of Mtb by all three MAIT cell clones (**Fig 6**), a different

273 trend compared to the response observed in the single *ΔribH1*, *ΔribH2* or double *ΔribH2*
274 *ΔribH1* Msm mutants. Furthermore, knockout of the gene *ribC* had no significant effect on T
275 cell recognition of Mtb.

276 **Fig 6. Differential impacts of riboflavin pathway knockouts on MR1T recognition of Mtb.**
277 The data represent the MR1T cell clone (1e4) IFN-γ response to DCs (1e4) infected at an MOI
278 of 10 of the indicated Mtb strain. The response for each Mtb strain was normalized to the
279 response of D454 H1-2, a classically restricted CD8 T cell clone that recognizes Mtb8.4 [22].
280 Data are representative of n=3 independent experiments. Statistical comparisons were
281 performed using a one-way ANOVA and Sidak's multiple comparison test whereby statistical
282 significance is represented by $p<0.05$, $p<0.001$, $p<0.0005$ $p<0.0001$, shown by *, **, ***, ****
283 respectively.

284 Discussion

285 In this study, we investigated the association between riboflavin biosynthesis and
286 MAIT cell activation by mycobacteria using strains of Msm or Mtb in which riboflavin
287 biosynthesis was blocked at the early (*ribA2* or *ribG*), penultimate (*ribA2* or *ribH*) or last step
288 of the pathway (*ribC*) (**Fig 1**). Deletion of *ribA2* or *ribG* blocks the production of 5-A-RU and
289 the downstream metabolites, DMRL and riboflavin, whereas loss of RibH function by deletion
290 of *ribH* in Mtb or *ribH1* and *ribH2* in Msm only blocks the production of DMRL and riboflavin,
291 whereas *ribC* deletion only blocks riboflavin production.

292 The riboflavin pathway produces both MAIT cell agonists and antagonists which differ
293 in terms of MR1 binding affinity and potency [23]. These include intermediates (F_0, DMRL)
294 and the end-product (riboflavin) of the pathway produced by enzyme-catalyzed reactions and
295 secondary metabolites formed by non-enzymatic reactions of pathway intermediates with
296 molecules from other pathways, which, in the case of Mtb, could include those derived from

297 the host (**Fig 7**). The level of activation of a given MR1T is therefore determined by its
298 selectivity for MR1 ligand recognition and balance between the level of agonists vs.
299 antagonists. While we have found that both F_0 and riboflavin are relatively weak antagonists
300 [8], it is possible that the metabolic state of the microbe could influence the relative proportion
301 of these ligands. The latter depends, in turn, on the metabolic state of the organism under the
302 conditions tested. For example, the level of the toxic aldehyde, methylglyoxal, produced
303 endogenously by Mtb [24] and also by host macrophages [25] from metabolites such as
304 dihydroxyacetone phosphate could influence the production of 5-A-RU derived ligands.
305 Likewise, an increased demand for F_{420} for persistence of Mtb under the conditions
306 encountered by Mtb during infection (hypoxia, oxidative stress, nitrosative stress) and/or under
307 drug pressure [18, 26] could drive the metabolic flux of 5-A-RU in mycobacteria towards the
308 production of deazaflavins at the expense of lumazine agonists. Therefore, the agonist/
309 antagonist balance, and the derangement thereof by perturbing the metabolic flux through the
310 biosynthetic pathway, could only be inferred indirectly by comparing the phenotypic readout
311 of MR1T activation by wildtype vs. mutant strains grown under standard *in vitro* culture, albeit
312 supplemented with riboflavin.

313 We observed both similarities and differences between the two mycobacterial species
314 in terms of the impact of riboflavin pathway disruption on MAIT cell activation. On the one
315 hand – and as observed in other microbes [7] – blocking the formation of 5-A-RU by disrupting
316 the pathway at an early stage had a major impact on MAIT cell activation, confirming the
317 centrality of this pathway intermediate for production of mycobacterial MR1T agonists.
318 Moreover, the profoundly reduced ability to recognize Msm incapable of producing 5-A-RU
319 applied equally to TRAV1-2+ and TRAV1-2- MR1Ts. However, residual MAIT cell activation
320 was observed for Msm Δ*ribA2*, Msm Δ*ribG* and Mtb Δ*ribA2* thus implicating an alternate
321 source/s of minor mycobacterial MAIT cell agonists distinct from the riboflavin pathway.

322 Furthermore, for both Msm and Mtb, activation of all MR1Ts tested was unaffected by
323 knockout of *ribC* which blocks the enzymatic route of DMRL metabolism to produce riboflavin
324 and 5-A-RU. On the other hand, deletion of *ribH* enhanced MAIT cell recognition of Mtb by
325 all three clones, D426-G11, D481-C7 and D481-F12 by 3-4-fold whereas in Msm, the
326 Δ*ribH2*Δ*ribH1* mutant was recognized as well as the parental wildtype by these clones. Thus,
327 blocking the enzymatic production of the MAIT cell agonist, DMRL, did not adversely affect
328 MAIT cell recognition in either Mtb or Msm, and paradoxically, enhanced it in Mtb, possibly
329 due to enhanced production of 5-A-RU-associated activating ligands. Conversely, this
330 phenotype was not recapitulated in Msm (**Fig 7**) [9]. That Msm also preferentially produces
331 lumazine antigens is suggested by the observation that the ablation of FbiC impacted the
332 recognition of Msm by the non-TRAV1-2 T cell clone D520 E10, which recognizes Msm and
333 not Mtb.

334 Other studies have demonstrated variable impacts of modulating flux through the
335 riboflavin biosynthetic pathway on MAIT cell activation. Using an alternative approach
336 involving overexpression rather than knockout of riboflavin pathway genes, Dey *et al*. also
337 observed marked differences between mycobacterial species [16]. In that study, Mtb *ribH*
338 overexpression modestly reduced activation of D426-G11, D481-C7 and D481-A9 by Mtb
339 CDC1551 but had the opposite effect in Msm, enhancing activation of these MR1Ts up to ~ 4-
340 fold in an MOI-dependent manner. Mtb *ribH* overexpression also enhanced by 9.3-fold the
341 activation of D426-G11 by *M. bovis* BCG, which, unlike Mtb and Msm (and for reasons that
342 are unclear) could not tolerate overexpression of *ribA2*, *ribG* and *ribF* [16]. In *S. typhimurium*
343 ST313 lineage 2 strains, evasion of MAIT cell recognition was shown to be attributable to
344 overexpression of DHBP synthase, which produces the second substrate for RibH [15].

345 In summary, the data presented herein support a central role for the riboflavin
346 pathway, and specifically 5-A-RU in generating a diverse array of mycobacterial ligands,

347 which in turn are associated with selective T cell recognition. The antigen 5-OP-RU was
348 initially described for both *E. coli*, and *Salmonella* species, and hence supported the concept
349 that MAIT cells were innate in their use of a highly conserved presentation molecule (MR1), a
350 conserved TCRα chain (TRAV1-2). However, in our previous work with both Msm and Mtb,
351 we have observed a diversity of both MR1-bound ligands and activating fractions [8].
352 Specifically, in our ongoing work we have not observed the lumazine antigens seen in Msm in
353 Mtb, and specifically note that we have not observed DMRL in both mycobacterial
354 specificities. While the failure to observe 5-OP-RU or DMRL could reflect their chemical
355 instability, it does not account for the diversity of ligands that we have observed. With regards
356 to TCR usage, we have found that the selective recognition of mycobacterial antigens is
357 associated with TCRβ chain usage [27]. Hence this work supports the hypothesis that further
358 identification of these antigens could be used to define the extent to which these T cell
359 responses are associated with infection with Mtb or could be harnessed for an improved
360 vaccine. We also note that while ablation of RibA2 has a profound effect on the recognition of
361 both Msm and Mtb, there were residual activating antigens in both these strains. Hence, it is
362 likely that there remain 5-A-RU-independent antigens yet to be discovered.
363
364 **Fig 7. MAIT cell agonists and antagonists produced via the riboflavin pathway in**
365 **mycobacteria.** Solid black arrows denote enzyme-catalyzed reactions. Dashed grey arrows
366 denote non-enzymatic reactions. MAIT cell agonists (green) or antagonists (red) are shown in
367 bold italics. RL, ribityllumazine. The production of photolumazines has only been observed in
368 Msm and not in Mtb [8] [9].

369 # Materials and methods

370 ## Media, culture conditions, strains, plasmids and chemicals

371 The plasmids used and constructs generated in this study are described in **S2 Table**. All strains
372 generated were derivatives of either *E. coli* DH5α, Msm mc^2 155 or Mtb H37RvMA, shown in
373 **S3 Table**. *E. coli* DH5α was grown in Luria-Bertani (LB) medium (10g/L tryptone, 5g/L yeast
374 extract and 10g/L NaCl) and plated onto Luria-Bertani agar (LB agar), containing LB media
375 components supplemented with 15g/L agar. Mycobacterial strains were grown in Middlebrook
376 7H9 OADC medium (4.7 g/L 7H9 (Millipore Sigma), 2g/L glycerol (Millipore Sigma), 2.5 ml
377 25% Tween 80, and 100 ml of oleic acid-albumin-dextrose-catalase (OADC) enrichment
378 (Millipore Sigma). Cells were plated onto Middlebrook 7H10 agar plates (19g/L 7H10
379 (Millipore Sigma), 100 ml OADC and 5 ml glycerol). Msm was grown in Erlenmeyer flasks in
380 a rotating incubator set at 100 rpm at 37°C and unless otherwise stated Mtb was cultured in
381 sealed cell culture flasks with no agitation at 37°C. Where required 7H9 broth or 7H10 solid
382 media was supplemented with 50 µg/ml kanamycin, 50 µg/ml hygromycin or 2.5 µg/ml
383 gentamicin. Riboflavin auxotrophs were supplemented with exogenous riboflavin at a
384 concentration of 83 µM for Msm or 21 µM for Mtb. Media used to select for knockout mutants
385 constructed by allelic exchange [28] or ORBIT [29] are described below.

386

387 ## Construction of mutant and complemented strains

388 Allelic exchange by homologous recombination was used to knockout *ribC* in Mtb and *ribC*,
389 *fbiC* and MSMEG_6598 in Msm, as described [28]. Briefly, 1000-2000 bp fragments amplified
390 up- and downstream of the gene of interest were ligated and cloned in p2NIL. The *Pac*I cassette
391 from either pGOAL19 or pGOAL17 cloned in the *Pac*I site in the p2NIL **(S2 Table).** The
392 resulting suicide construct was electroporated into the mycobacterial strain and single

393 crossover clones selected by plating onto 7H10 media supplemented with 50 µg/ml kanamycin,
394 50 µg/ml hygromycin and 40 µg/ml X-gal (for pGOAL19 constructs) or 50 µg/ml kanamycin
395 and 40 µg/ml X-gal (for pGOAL17 constructs). Double crossover recombinants were selected
396 by plating onto media supplemented with 2% sucrose, 40 µg/ml X-gal and riboflavin at
397 concentration of 83 µM for Msm or 21 µM for Mtb. The ORBIT system [29] was used to create
398 individual gene knockouts of *ribA2*, *ribG* or *ribH* in Msm and *ribA2* or *ribH* in Mtb. Briefly, a
399 targeting oligonucleotide containing 70 bp of homology to the target gene flanked by the BxbI
400 phage *attP* sequence **(S4 Table)** was co-electroporated with pKM464 into the mycobacterial
401 strain carrying pKM461 and selected on 7H10 agar containing 10% sucrose and 50 µg/ml
402 hygromycin. To create complementation vectors, ca. 300-400 bp upstream of the gene along
403 with its open reading frame were amplified and cloned into an integrating vector. All primers
404 and amplicons are described in **S4 Table**. The complementation vectors were introduced into
405 the knockout mutants by electroporation and selected on the appropriate antibiotic selection
406 plates. DNA was extracted from all gene knockout and complement strains using the CTAB
407 method [30] and the gene deletion/ gene restoration verified by whole genome sequencing.
408

409 # RNA extraction

410 Mtb and Msm strains were inoculated in 80 ml of Middlebrook 7H9 OADC broth
411 supplemented with 0.01% tyloxapol until mid-log phase (OD_{600} between 0.4 and 0.6) was
412 reached. Media was supplemented with riboflavin as necessary. Afterwards, cells were
413 pelleted, resuspended in 1 ml of TriZOL (Thermo Scientific) and 5 µl of glycogen (Thermo
414 Scientific) and then transferred to screw-cap homogenization microtubes prefilled with Lysing
415 Matrix B (MP Biomedical). The cells were homogenized using the FastPrep-24 bead beater
416 (MP Biomedical) at 6 m/s for 30 seconds (6 rounds), cooling on ice for 2 min between cycles.
417 After centrifugation at 12,000×*g* for 120s, homogenate was collected in a new tube and treated

418 with 200 µl of chloroform followed by vortexing for 15 seconds and incubation at room
419 temperature for 5 minutes. Samples were centrifuged at 12,000×*g* for 15 minutes at 4ºC and
420 upper aqueous phase was transferred into new tubes containing 500 µl of cold isopropanol for
421 overnight precipitation. Samples were centrifuged at 12,000×*g* for 10 min and supernatant
422 disposed. Pellet was washed with 1 ml of cold 80% ethanol and then resuspended with nuclease
423 free water. Extracted RNA was processed for DNase treatment and clean-up using the RNeasy
424 Mini Kit (QIAGEN) and RNase free DNase Set (QIAGEN) according to manufacturer's
425 instruction to eliminate genomic DNA. RNA was quantified using a NanoDrop (Thermo
426 Scientific) and Agilent TapeStation.
427

428 ## Gene expression analysis

429 Two hundred ng of RNA was retrotranscribed to complementary DNA (cDNA) using the
430 SuperScript IV VILO Master Mix (Thermo Scientific) according to manufacturer's instruction.
431 PowerTrack SYBR green Master Mix (Thermo Scientific) with 250 nM of primer pair was
432 used to amplify the target region of interest for 5 ng of cDNA following manufacturer's
433 instruction. Quantification was run on the QuantStudio 3 Real-Time PCR System (Thermo
434 Scientific). A no reverse transcriptase (no-RT) control was included for all samples to ensure
435 that there was no genomic DNA contamination. Amplicon size was confirmed by melting
436 curves for each sample. All qRT-PCR experiments were performed with two technical
437 replicates derived from three biological replicates for Mtb and two biological replicates for
438 Msm. Transcript levels of the target genes were normalized to the housekeeping gene *sigA* and
439 calibrated to wildtype Mtb and Msm to calculate the ΔΔCt and determine fold difference in
440 gene expression. The primers used are listed in **S5 Table**.
441

442 # Growth kinetics of mycobacteria

443 Msm and Mtb growth kinetics in 7H9 media were monitored by OD_{600} as previously described
444 [17].
445

446 ## Growth of Mtb and Msm for untargeted and targeted proteomics

447 Glycerol stocks of Mtb and Msm strains were used to start cultures on 7H11 agar plates
448 (Millipore Sigma, Cat No.: M0428) supplemented with the appropriate antibiotics with or
449 without riboflavin. Plates were incubated for 2 weeks for Mtb and 4 to 5 days for Msm at 37ºC.
450 Cells were scraped from plates into 7H9 media supplemented with OADC with or without
451 riboflavin and grown at 37ºC until mid-log phase. Mtb cells from all strains were inactivated
452 by γ-irradiation and inactivation was confirmed using the Alamar Blue assay. Cells were
453 harvested and washed 3 times either with phosphate buffered saline (PBS) or water to remove
454 media and stored at -80ºC until further processing. Cell pellets were further processed as
455 previously described [17].
456

457 # Liquid chromatography - MS/MS analysis

458 Thirty µg of retentate from whole cell lysate from Msm and Mtb after ultrafiltration with 3 kDa
459 filters (Millipore Sigma, Product Number: UFC9003), was subjected to in-gel trypsin digestion
460 as described previously [31]. Digested samples were resuspended in 120 µl of loading buffer
461 (3% acetonitrile, 0.1% formic acid in water). All samples were analyzed using nano-UHPLC
462 (ultrahigh-pressure liquid chromatography) nanoElute (Bruker Daltonics, USA) coupled to a
463 timsTOF Pro (Bruker Daltonics, USA) mass spectrometer. 0.25 µg of total peptides were
464 loaded onto a trap cartridge using PepMap™ Neo Trap Cartridge (Thermo Scientific, Cat:
465 174500) (5 µm C18 300 µm X 5 mm) packed with spherical, fully porous, ultrapure silica and

466 reverse phase UHPLC was performed in a PepSep Ten Column (Bruker Daltonics, Part
467 No:1895802) (1.5 µm C18 75 µm X 25 cm). Mobile phase A was 0.1% formic acid in water;
468 mobile phase B was 0.1% formic acid in acetonitrile. Liquid chromatography (LC) separation
469 was carried out at a flow rate of 0.5 µL/min using a linear gradient of 5% solvent B to 30%
470 solvent B over a duration 17.8 minutes, then 30% solvent B to 95% solvent B for 2.5 minutes.
471 Thereafter, 95% solvent B was held for 2.4 minutes for equilibration.

472 Mass spectra and tandem mass spectra were obtained using the parallel accumulation
473 serial fragmentation (PASEF) acquisition method in positive ion mode. Captive spray source
474 was operated with the following settings: 1600 V capillary voltage, 3.0 l/min of dry gas at
475 200ºC with the NanoBooster switched off.

476 A SWATH-MS spectral library was generated by analyzing samples using data-
477 dependent acquisition (DDA-PASEF). DDA was set to obtain high resolution MS scans over
478 the m/z range from 100 to 1700 and ion mobility range from 0.70 Vs/cm^2 to 1.50 Vs/cm^2. Ramp
479 time was set at 100 msec and accumulation time was set at 100 msec. The collision energy was
480 set to follow a linear function starting from 20 eV for 0.6 V. s/cm^2 to 59 eV for 1.6 V. s/cm^2.
481 The number of PASEF MS/MS was set to 6. For DIA-PASEF analysis, data was acquired with
482 a method consisting of 24 mass steps per cycle **(S6 Table)**. Mass width was set at 50 Da with
483 1 Da overlap between windows covering a mass range between 307.8 to 1484.8 Da. The ion
484 mobility range ($1/K_0$) covered was between 0.71 to 1.44. The collision energy was set to follow
485 a linear function starting from 20 eV for 0.6 V. s/cm^2 to 59 eV for 1.6 V. s/cm^2.
486

487 # Untargeted proteomics analysis by Data Independent Acquisition
488 # (DIA)

489 DIA-PASEF data was processed on FragPipe software v. 19.1 (MSFragger version 3.7,
490 IonQuant version 1.8.10, Philosopher version 4.8.1) using the DIA_SpecLib-Quant workflow
491 as described [32]. DIA raw files were loaded with DIA Quant selected as data type while DDA
492 raw files were loaded for spectral library generation. A search was conducted using default
493 settings with the FASTA sequence obtained from the Mycobrowser database (Release 4, 2021-
494 03-23). Decoy and contaminant sequences were generated by FragPipe. Default settings of
495 MSFragger was used, supplemented with oxidation of M (+ 15.9949 Da mass shift) acetylation
496 at N-terminal (+ 42.0106) as variable modifications. Advanced output options were set to write
497 calibrated mzML and MGF files. Tryptic searches were performed with 20 ppm precursor and
498 fragment tolerance permitting up to 2 missed cleavages. Search results were filtered to 1% FDR
499 at both protein and peptide levels using peptide prophet. Output files with quantification based
500 on summed intensity of all ions for a single peptide and summed intensity of peptides for a
501 single protein were generated. The output file containing summed intensity of peptides for a
502 single protein was used for quantification of proteins and is provided in **S6 Table.**
503

504 # Targeted proteomics analysis by parallel reaction monitoring -
505 # PASEF Mass Spectrometry (PRM-PASEF MS)

506 DDA peptide search results from MSFragger version 3.7 were used to build a spectral library
507 in Skyline [33]. The Ion Mobility library was generated on Skyline software from raw DDA
508 files. The protein list was trimmed to contain only proteins from the riboflavin biosynthetic
509 pathway. Tryptic peptides were filtered to have length only be between 8 and 30 amino acids.

510 Tryptic peptides containing C, M, D-P, and W were excluded. Peptides for each protein were
511 further screened based on the shape of the precursor chromatogram and absence of the
512 precursor peak from the cognate knock-out sample. Ion types were limited to only precursor
513 ions (2 and 3 ion charges) and 6 y ions (1 and 2 ion charges). The retention time window was
514 set at 3 minutes and mass accuracy set at 10 ppm for both MS1 and MS2 filtering. The method
515 was exported to timsTOF engine (Bruker Daltonics, USA) as an unscheduled method. 0.25 µg
516 of each Mtb sample was loaded for reverse phase UHPLC and MS. performed. Analytical
517 settings were kept the same as previously described (LC-MS/MS Section) with the inclusion
518 of a target list containing the Mtb peptides to quantify in the PRM-PASEF method generated.
519
520 Raw data was exported into Skyline software and peptides with the best peak shape and
521 intensity were selected for further optimization. At least, one peptide per protein was selected
522 for the final method. For absolute quantification, peptides labeled with heavy C-terminal
523 Lysine (K) or Arginine (R) were purchased (Biosynth Ltd, UK) to be used as internal standards.
524 Limit of detection (LOD) and Limit of quantification (LOQ) were calculated using a linear
525 regression method as described elsewhere [34]. Details of the peptide sequences and transition
526 list used for the PRM-PASEF experiment are shown in **Table S7**.
527

528 Absolute quantification of riboflavin pathway proteins by PRM-
529 PASEF MS

530 A mix of the heavy labeled peptides containing 10^{-1} – 10^{-5} pmol/µl of each peptide was used
531 to resuspend each of the digested samples at a final concentration of 250 ng/µl of digested
532 protein **(S8 Table)**. After resuspension, the sample peptide concentration was estimated using
533 a Nanodrop 1000c and the concentration was adjusted to ensure equal loading of all samples.

534 The developed PRM-PASEF MS method was exported as a scheduled method and used to
535 obtain the Ratio to Heavy Standard for each of the monitored peptides. Briefly, raw data from
536 each injection was imported into Skyline [33] and peak boundaries for each peptide were
537 manually validated and adjusted if necessary. The Ratio to Heavy Standard for each peptide as
538 calculated by Skyline was exported into Prism GraphPad for statistical analysis.
539

540 Whole genome sequencing

541 Genomic DNA was analyzed at the Genomics and Microarray Core at the University of
542 Colorado Anschutz using a NovaSEQ 6000 Instrument, paired end 150 cycles 2x150. Reads
543 were subjected to quality control using FastQC before and after trimming. Trimming was
544 performed using trimmomatic. Alignment of reads to the Mtb H37Rv genome (NC_000962.3)
545 or Msm mc^2 155 (CP000480.1)/ (NZ_CP054795.1) was performed using Bowtie2. Due to the
546 high density of reads, the aligned sam files were subjected to subsample using samtools.
547 Samtools were also used to determine coverage results. Subsample alignment was used to
548 determine SNPs using lofreq with a minimum coverage of 10 and minimum frequency of 80.
549 The bam file was visualized using the Geneious software. The expected deleted regions were
550 confirmed by visual inspection and very few inadvertent second-site mutations were detected
551 in the deletion mutants of Msm and Mtb relative to their parental wildtype strains (**Table S9A,**
552 **B1, B2 and B3**).
553

554 T cell clones

555 All T cell clones were expanded and maintained as previously described [4, 22]. Five T cell
556 clones were used in this work. All have been published previously: D426 G11, D481 C7, D481
557 F12 - MAIT cell clones expressing TRAV1-2 [4, 8]; D520 E10 is a MR1-restricted T cell

558 clone expressing TRAV19-1[8], and D454 H1-2 is a CD8 T cell clone that recognizes
559 Mtb8.433-43 and is restricted by HLA-B*15:01 [22] (see **S9 Table** for details of TCRs).
560

561 # IFN-γ ELISpot assays

562 All Msm and Mtb strains were grown in the presence of riboflavin with or without supplements
563 as needed (see above) to an OD_{600} ~ 0.5 and frozen down. For all ELISPOT assays, ELISPOT
564 plates were coated with anti-IFN-γ antibody (Mabtech, clone 1-D1K, Cat No. 3420-3-1000,
565 used at 10 μg/ml) as previously described [35]. After overnight incubation at 4°C, ELISPOT
566 plates were washed three times with phosphate-buffered saline and then blocked with RPMI
567 1640 + 10% human serum for at least 1 hour. For experiments with Msm approximately $1x10^4$
568 DC were plated in the ELISPOT wells in RPMI+10% HuS. Msm bacilli were added to the
569 wells at concentrations indicated for each experiment. PHA was used as positive control. After
570 at least 1 hour, $1\text{-}2x10^4$ T cell clones were added, and the plate was incubated overnight at
571 37°C. IFN-γ ELISPOTs were enumerated following development as previously described [35].
572 For experiments with live Mtb, 5×10^5 DC were plated in each well of an ultralow adherence
573 24 well tissue culture plate. Mtb was added at the MOI indicated and incubated overnight.
574 $1x10^4$ DC were plated in the ELISPOT wells in RPMI+10% HuS. $1\text{-}2x10^4$ T cell clones were
575 added, and the plate was incubated overnight at 37°C. IFN-γ ELISPOTs were enumerated
576 following development.
577

578 # Statistical analysis

579 Statistical analysis was conducted by one-way ANOVA and either Sidak's or Dunnett's
580 multiple comparison test. Statistically significant difference applied is stipulated in the figure
581 legend. Statistical calculations were performed using GraphPad Prism 10 statistical software

582 (GraphPad Software, Inc., San Diego, CA). For proteomics, qRT-PCR and the EliSPOT assay,
583 statistical comparisons were performed using a one-way ANOVA followed by Dunnett's or
584 Sidak's multiple comparison test. These analyses were performed using GraphPad Prism 9 and
585 statistical significance was established at $p < 0.05$.
586

587 # Acknowledgements

588 This research was supported by an Oppenheimer Fellowship from the Oppenheimer Memorial
589 Trust (to V.M.; www.omt.org.za), and grants from the Bill and Melinda Gates Foundation INV-
590 004757 (to V.M.; www.gatesfoundation.org), the Broad Institute (to V.M.;
591 www.broadinstitute.org), the South African Medical Research Council (to V.M.;
592 www.samrc.ac.za), the Department of Science and Innovation and National Research
593 Foundation of South Africa (to V.M.; www.nrf.ac.za), the National Institutes of Health (NIH;
594 www.niaid.nih.gov) R01AI147954 (to E.J.A., W.H. and D.M.L., MPIs), AWD100279 (to
595 K.M.D. and C.M.), and internal funds from Colorado State University (to K.M.D.). The funders
596 had no role in study design, data collection and analysis, decision to publish, or preparation of
597 the manuscript.

598 # Author contributions

599 Conceptualization: Melissa Chengalroyen, Karen Dobos, David Lewinsohn, Deborah
600 Lewinsohn, Valerie Mizrahi, Digby Warner

601 Data curation: Nurudeen Oketade, Melissa Chengalroyen, Gwendolyn Swarbrick

Formal analysis: Nurudeen Oketade, Carolina Mehaffy, Gwendolyn Swarbrick, Melissa Chengalroyen

Funding acquisition: Valerie Mizrahi, David Lewinsohn, Karen Dobos, Deborah Lewinsohn, Erin Adams, William Hildebrand

Investigation: Melissa Chengalroyen, Nurudeen Oketade, Gwendolyn Swarbrick, Carolina Mehaffy, Aneta Worley, Mabule Raphela, Megan Lucas

Methodology: Nurudeen Oketade, Gwendolyn Swarbrick, Luisa Nieto Ramirez, Carolina Mehaffy, Melissa Chengalroyen, Karen Dobos, David Lewinsohn, Valerie Mizrahi

Project administration: Melissa Chengalroyen, Carolina Mehaffy, Nurudeen Oketade, Gwendolyn Swarbrick, Karen Dobos, David Lewinsohn, Valerie Mizrahi

Resources: Valerie Mizrahi, Karen Dobos, David Lewinsohn

Supervision: Luisa Nieto Ramirez, Melissa Chengalroyen, Digby Warner, Valerie Mizrahi, Karen Dobos, Deborah Lewinsohn, David Lewinsohn

Validation: Melissa Chengalroyen, Nurudeen Oketade, Gwendolyn Swarbrick

Visualization: Nurudeen Oketade, Gwendolyn Swarbrick, Melissa Chengalroyen, Carolina Mehaffy, Valerie Mizrahi

Writing – original draft: Melissa Chengalroyen, David Lewinsohn, Nurudeen Oketade, Valerie Mizrahi

Writing – review & editing: Melissa Chengalroyen, Nurudeen Oketade, Luisa Nieto Ramirez, Megan Lucas, Karen Dobos, David Lewinsohn, Valerie Mizrahi

622 # References

623 1. Huang S, Gilfillan S, Cella M, Miley MJ, Lantz O, Lybarger L, et al. Evidence for
624 MR1 antigen presentation to mucosal-associated invariant T cells. J Biol Chem.
625 2005;280(22):21183-93.

626 2. Treiner E, Duban L, Moura IC, Hansen T, Gilfillan S, Lantz O. Mucosal-associated
627 invariant T (MAIT) cells: an evolutionarily conserved T cell subset. Microbes Infect.
628 2005;7(3):552-9.

629 3. Sharma PK, Wong EB, Napier RJ, Bishai WR, Ndung'u T, Kasprowicz VO, et al.
630 High expression of CD26 accurately identifies human bacteria-reactive MR1-restricted
631 MAIT cells. Immunology. 2015;145(3):443-53.

632 4. Gold MC, Cerri S, Smyk-Pearson S, Cansler ME, Vogt TM, Delepine J, et al. Human
633 Mucosal Associated Invariant T Cells Detect Bacterially Infected Cells. PLOS Biology.
634 2010;8(6):e1000407.

635 5. Le Bourhis L, Martin E, Peguillet I, Guihot A, Froux N, Core M, et al. Antimicrobial
636 activity of mucosal-associated invariant T cells. Nat Immunol. 2010;11(8):701-8.

637 6. Kjer-Nielsen L, Patel O, Corbett AJ, Le Nours J, Meehan B, Liu L, et al. MR1
638 presents microbial vitamin B metabolites to MAIT cells. Nature. 2012;491(7426):717-23.

639 7. Corbett AJ, Eckle SB, Birkinshaw RW, Liu L, Patel O, Mahony J, et al. T-cell
640 activation by transitory neo-antigens derived from distinct microbial pathways. Nature.
641 2014;509(7500):361-5.

642 8. Harriff MJ, McMurtrey C, Froyd CA, Jin H, Cansler M, Null M, et al. MR1 displays
643 the microbial metabolome driving selective MR1-restricted T cell receptor usage. Sci
644 Immunol. 2018;3(25).

645 9. Krawic JR, Ladd NA, Cansler M, McMurtrey C, Devereaux J, Worley A, et al.
646 Multiple Isomers of Photolumazine V Bind MR1 and Differentially Activate MAIT Cells. J
647 Immunol. 2024;212(6):933-40.

648 10. Meermeier EW, Laugel BF, Sewell AK, Corbett AJ, Rossjohn J, McCluskey J, et al.
649 Human TRAV1-2-negative MR1-restricted T cells detect S. pyogenes and alternatives to
650 MAIT riboflavin-based antigens. Nat Commun. 2016;7:12506.

651 11. Chen Z, Wang H, D'Souza C, Sun S, Kostenko L, Eckle SB, et al. Mucosal-associated
652 invariant T-cell activation and accumulation after in vivo infection depends on microbial
653 riboflavin synthesis and co-stimulatory signals. Mucosal Immunol. 2017;10(1):58-68.

654 12. Legoux F, Bellet D, Daviaud C, El Morr Y, Darbois A, Niort K, et al. Microbial
655 metabolites control the thymic development of mucosal-associated invariant T cells. Science.
656 2019;366(6464):494-9.

657 13. Hartmann N, McMurtrey C, Sorensen ML, Huber ME, Kurapova R, Coleman FT, et
658 al. Riboflavin Metabolism Variation among Clinical Isolates of Streptococcus pneumoniae
659 Results in Differential Activation of Mucosal-associated Invariant T Cells. Am J Respir Cell
660 Mol Biol. 2018;58(6):767-76.

661 14. Jahreis S, Bottcher S, Hartung S, Rachow T, Rummler S, Dietl AM, et al. Human
662 MAIT cells are rapidly activated by Aspergillus spp. in an APC-dependent manner. Eur J
663 Immunol. 2018;48(10):1698-706.

664 15. Preciado-Llanes L, Aulicino A, Canals R, Moynihan PJ, Zhu X, Jambo N, et al.
665 Evasion of MAIT cell recognition by the African Salmonella Typhimurium ST313 pathovar
666 that causes invasive disease. Proc Natl Acad Sci U S A. 2020;117(34):20717-28.

667 16. Dey RJ, Dey B, Harriff M, Canfield ET, Lewinsohn DM, Bishai WR. Augmentation
668 of the Riboflavin-Biosynthetic Pathway Enhances Mucosa-Associated Invariant T (MAIT)
669 Cell Activation and Diminishes Mycobacterium tuberculosis Virulence. mBio.
670 2021;13(1):e0386521.

671 17. Chengalroyen MD, Mehaffy C, Lucas M, Bauer N, Raphela ML, Oketade N, et al.
672 Modulation of riboflavin biosynthesis and utilization in mycobacteria. Microbiol Spectr.
673 2024:e0320723.

674 18. Grinter R, Greening C. Cofactor F420: an expanded view of its distribution,
675 biosynthesis and roles in bacteria and archaea. FEMS Microbiol Rev. 2021;45(5).

676 19. Macheroux P, Kappes B, Ealick SE. Flavogenomics--a genomic and structural view
677 of flavin-dependent proteins. FEBS J. 2011;278(15):2625-34.

678 20. Selengut JD, Haft DH. Unexpected abundance of coenzyme F(420)-dependent
679 enzymes in Mycobacterium tuberculosis and other actinobacteria. J Bacteriol.
680 2010;192(21):5788-98.

681 21. Kis K, Kugelbrey K, Bacher A. Biosynthesis of riboflavin. The reaction catalyzed by
682 6,7-dimethyl-8-ribityllumazine synthase can proceed without enzymatic catalysis under
683 physiological conditions. J Org Chem. 2001;66(8):2555-9.

684 22. Lewinsohn DA, Winata E, Swarbrick GM, Tanner KE, Cook MS, Null MD, et al.
685 Immunodominant tuberculosis CD8 antigens preferentially restricted by HLA-B. PLoS
686 Pathog. 2007;3(9):1240-9.

687 23. Eckle SB, Corbett AJ, Keller AN, Chen Z, Godfrey DI, Liu L, et al. Recognition of
688 Vitamin B Precursors and Byproducts by Mucosal Associated Invariant T Cells. J Biol Chem.
689 2015;290(51):30204-11.

690 24. Pethe K, Sequeira PC, Agarwalla S, Rhee K, Kuhen K, Phong WY, et al. A chemical
691 genetic screen in Mycobacterium tuberculosis identifies carbon-source-dependent growth
692 inhibitors devoid of in vivo efficacy. Nat Commun. 2010;1(5):57.

693 25. Rachman H, Kim N, Ulrichs T, Baumann S, Pradl L, Nasser Eddine A, et al. Critical
694 role of methylglyoxal and AGE in mycobacteria-induced macrophage apoptosis and
695 activation. PLoS One. 2006;1(1):e29.

696 26. Darwin KH, Ehrt S, Gutierrez-Ramos JC, Weich N, Nathan CF. The proteasome of
697 Mycobacterium tuberculosis is required for resistance to nitric oxide. Science.
698 2003;302(5652):1963-6.

699 27. Narayanan GA, Nellore A, Tran J, Worley AH, Meermeier EW, Karamooz E, et al.
700 Alternative splicing of MR1 regulates antigen presentation to MAIT cells. Sci Rep.
701 2020;10(1):15429.

702 28. Gopinath K, Warner DF, Mizrahi V. Targeted gene knockout and essentiality testing
703 by homologous recombination. Methods Mol Biol. 2015;1285:131-49.

704 29. Murphy KC, Nelson SJ, Nambi S, Papavinasasundaram K, Baer CE, Sassetti CM.
705 ORBIT: a New Paradigm for Genetic Engineering of Mycobacterial Chromosomes. mBio.
706 2018;9(6).

30. van Soolingen D, Hermans PW, de Haas PE, Soll DR, van Embden JD. Occurrence and stability of insertion sequences in Mycobacterium tuberculosis complex strains: evaluation of an insertion sequence-dependent DNA polymorphism as a tool in the epidemiology of tuberculosis. J Clin Microbiol. 1991;29(11):2578-86.

31. Mehaffy C, Lucas M, Kruh-Garcia NA, Dobos KM. Methods for Proteomic Analyses of Mycobacteria. In: Parish T, Kumar A, editors. Mycobacteria Protocols. New York, NY: Springer US; 2021. p. 533-48.

32. Yu F, Teo GC, Kong AT, Frohlich K, Li GX, Demichev V, et al. Analysis of DIA proteomics data using MSFragger-DIA and FragPipe computational platform. Nat Commun. 2023;14(1):4154.

33. MacLean B, Tomazela DM, Shulman N, Chambers M, Finney GL, Frewen B, et al. Skyline: an open source document editor for creating and analyzing targeted proteomics experiments. Bioinformatics. 2010;26(7):966-8.

34. Mehaffy C, Dobos KM, Nahid P, Kruh-Garcia NA. Second generation multiple reaction monitoring assays for enhanced detection of ultra-low abundance Mycobacterium tuberculosis peptides in human serum. Clin Proteomics. 2017;14:21.

35. Heinzel AS, Grotzke JE, Lines RA, Lewinsohn DA, McNabb AL, Streblow DN, et al. HLA-E-dependent presentation of Mtb-derived antigen to human CD8+ T cells. J Exp Med. 2002;196(11):1473-81.

Supporting information

S1 Fig. Schematic representation of the genomic loci of the riboflavin biosynthesis pathway mutants of Msm (left) and Mtb (right). Deletion mutants constructed by ORBIT carry a vector sequence which include a *hyg* resistance marker whereas the allelic exchange mutants are unmarked.

S2 Fig. **Growth phenotyping on solid media.** Growth of Msm (Left) and Mtb (right) riboflavin pathway mutants and complemented counterparts assessed by streaking on Middlebrook 7H10 with or without riboflavin (RF) supplement. Riboflavin supplement was used at a concentration of 83 μM for culturing Msm, or 21 μM for Mtb.

S3 Fig. Protein abundance of Mtb strains assessed by PRM. Stable isotope-labeled standard (SIS) peptides were selected for selected riboflavin pathway genes for targeted quantification of proteins using LC-MS) Ratio to heavy standard represents protein

739 abundance of RibC **(A)**, and RibH **(B and C)** in different strains of Mtb. Data are shown as
740 mean quantification ± SEM of three biological replicates relative to Mtb wildtype (WT).
741 Statistical comparisons were performed using a one-way ANOVA and Sidak's multiple
742 comparison test whereby statistical significance is represented by $p<0.05$, $p<0.001$, $p<0.0005$
743 $p<0.0001$, shown by *, **, ***, **** respectively. ns, not significant.

744 **S4 Fig. Recognition of D520 E10 by Mtb.** The data represent the MR1T cell clone (1e4)
745 IFN-γ response to DCs (1e4) infected at an MOI of 10 of with wildtype Mtb or in response to
746 the positive control, PHA. Data are representative of n=3 independent experiments.

747

748 **S1 Table. TCR sequence of MR1T cell clones**

749 **S2 Table**. **Plasmids used in this study**

750 **S3 Table. Strains used in this study**

751 **S4 Table. Oligonucleotides used to create knockouts and complemented strains**

752 **S5 Table. Primers used for qRT-PCR analysis**

753 **S6 Table. Window scheme used for DIA-PASEF acquisition**

754 **S7 Table. Peptides used for targeted proteomics by PRM-MS**

755 **S8 Table. Peptides used for targeted proteomics by PRM-MS and concentration used in**
756 **final assay**

757 **S9A Table. Confirmation of riboflavin pathway mutants by WGS**

758 **S9B Tables. SNPs detected in Msm knockout mutants compared to wildtype**

759 **S9 B1 & B2 Tables. SNPs detected in Msm mutants and not in wildtype**

760 **S9 B3 Table. SNPs detected in Mtb mutants and not in wildtypee**

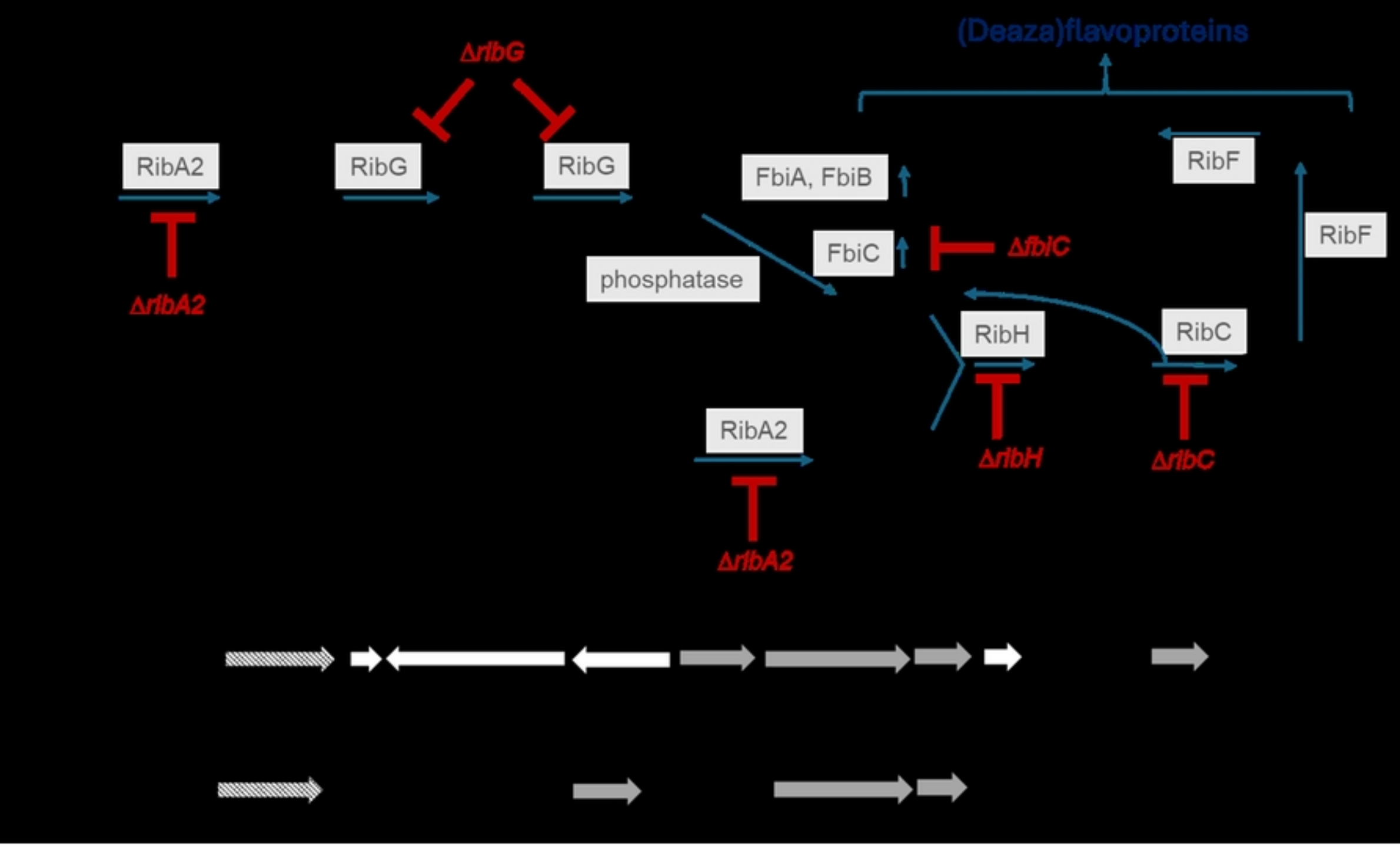
(Deaza)flavoproteins
ΔribG
RibA2
RibG
RibG
FbiA, FbiB
RibF
RibF
FbiC
ΔfbiC
phosphatase
ΔribA2
RibH
RibC
RibA2
ΔribH
ΔribC
ΔribA2

Figure 1

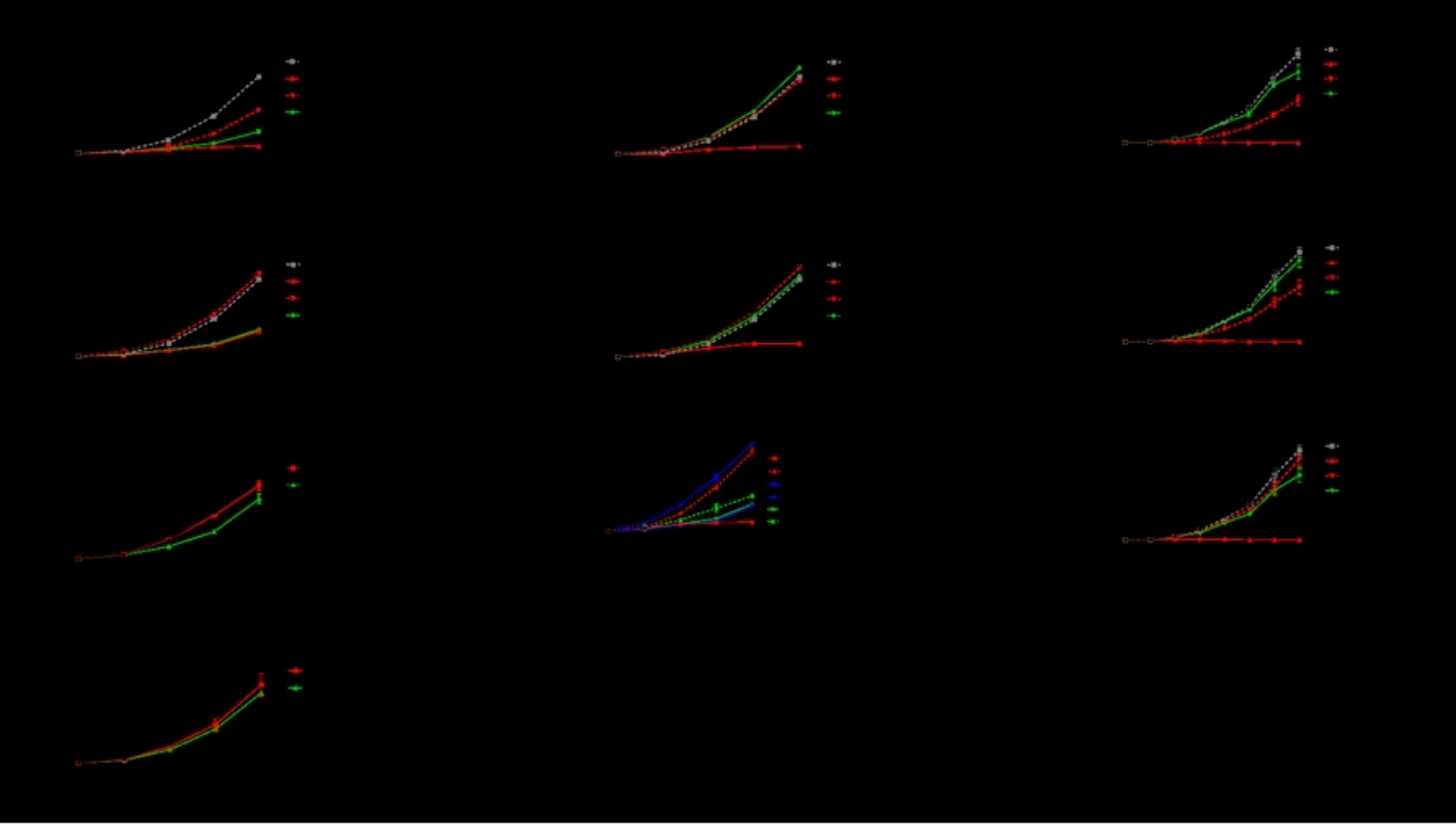

Figure 2

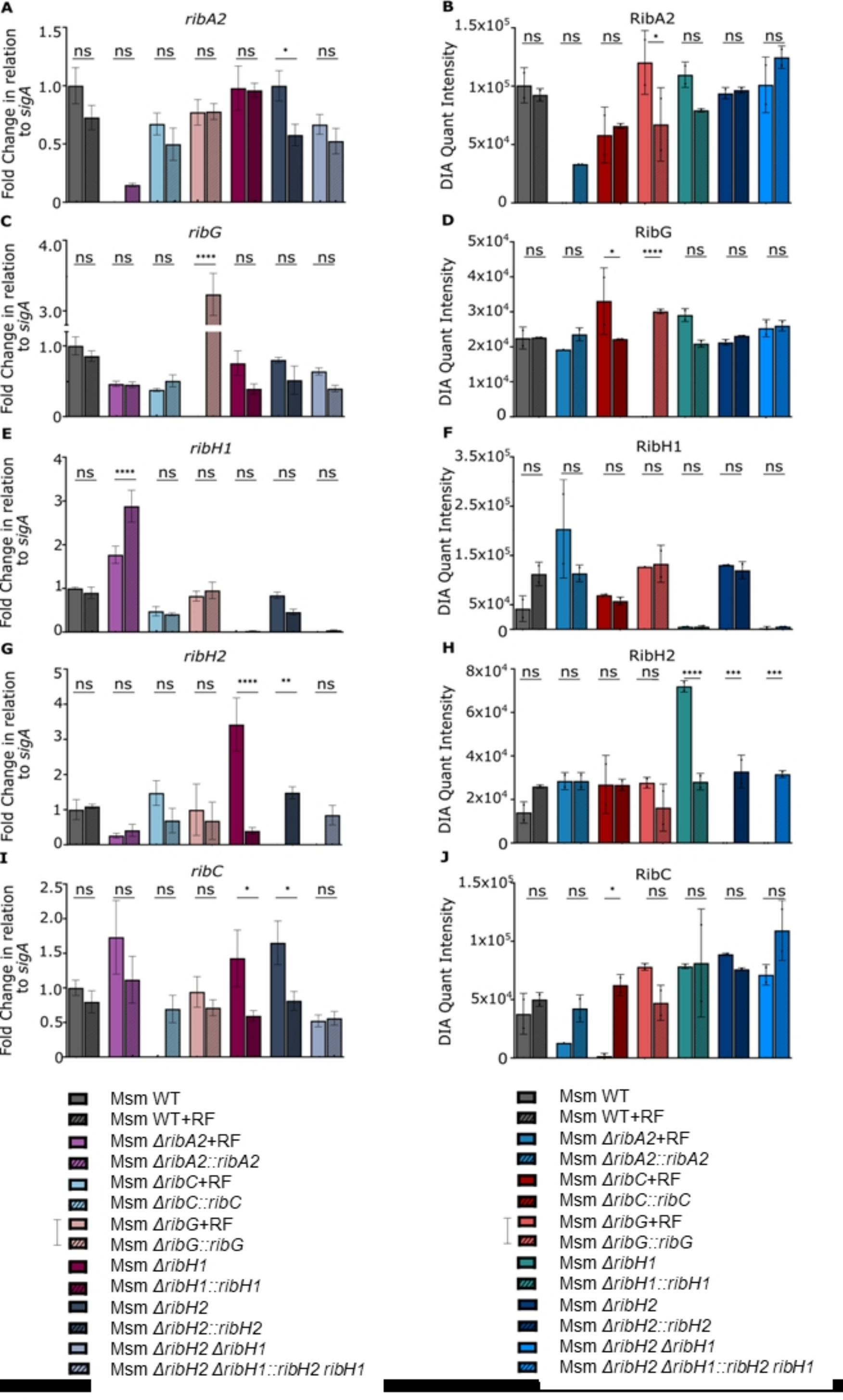
A
ribA2
Fold Change in relation to sigA
ns ns ns ns ns * ns
B
RibA2
DIA Quant Intensity
ns ns ns * ns ns ns
C
ribG
Fold Change in relation to sigA
ns ns ns **** ns ns ns
D
RibG
DIA Quant Intensity
ns ns * **** ns ns ns
E
ribH1
Fold Change in relation to sigA
ns **** ns ns ns ns ns
F
RibH1
DIA Quant Intensity
ns ns ns ns ns ns ns
G
ribH2
Fold Change in relation to sigA
ns ns ns ns **** ** ns
H
RibH2
DIA Quant Intensity
ns ns ns ns **** *** ***
I
ribC
Fold Change in relation to sigA
ns ns ns ns * * ns
J
RibC
DIA Quant Intensity
ns ns * ns ns ns ns
Msm WT
Msm WT+RF
Msm ΔribA2+RF
Msm ΔribA2::ribA2
Msm ΔribC+RF
Msm ΔribC::ribC
Msm ΔribG+RF
Msm ΔribG::ribG
Msm ΔribH1
Msm ΔribH1::ribH1
Msm ΔribH2
Msm ΔribH2::ribH2
Msm ΔribH2 ΔribH1
Msm ΔribH2 ΔribH1::ribH2 ribH1
Msm WT
Msm WT+RF
Msm ΔribA2+RF
Msm ΔribA2::ribA2
Msm ΔribC+RF
Msm ΔribC::ribC
Msm ΔribG+RF
Msm ΔribG::ribG
Msm ΔribH1
Msm ΔribH1::ribH1
Msm ΔribH2
Msm ΔribH2::ribH2
Msm ΔribH2 ΔribH1
Msm ΔribH2 ΔribH1::ribH2 ribH1

Figure 3

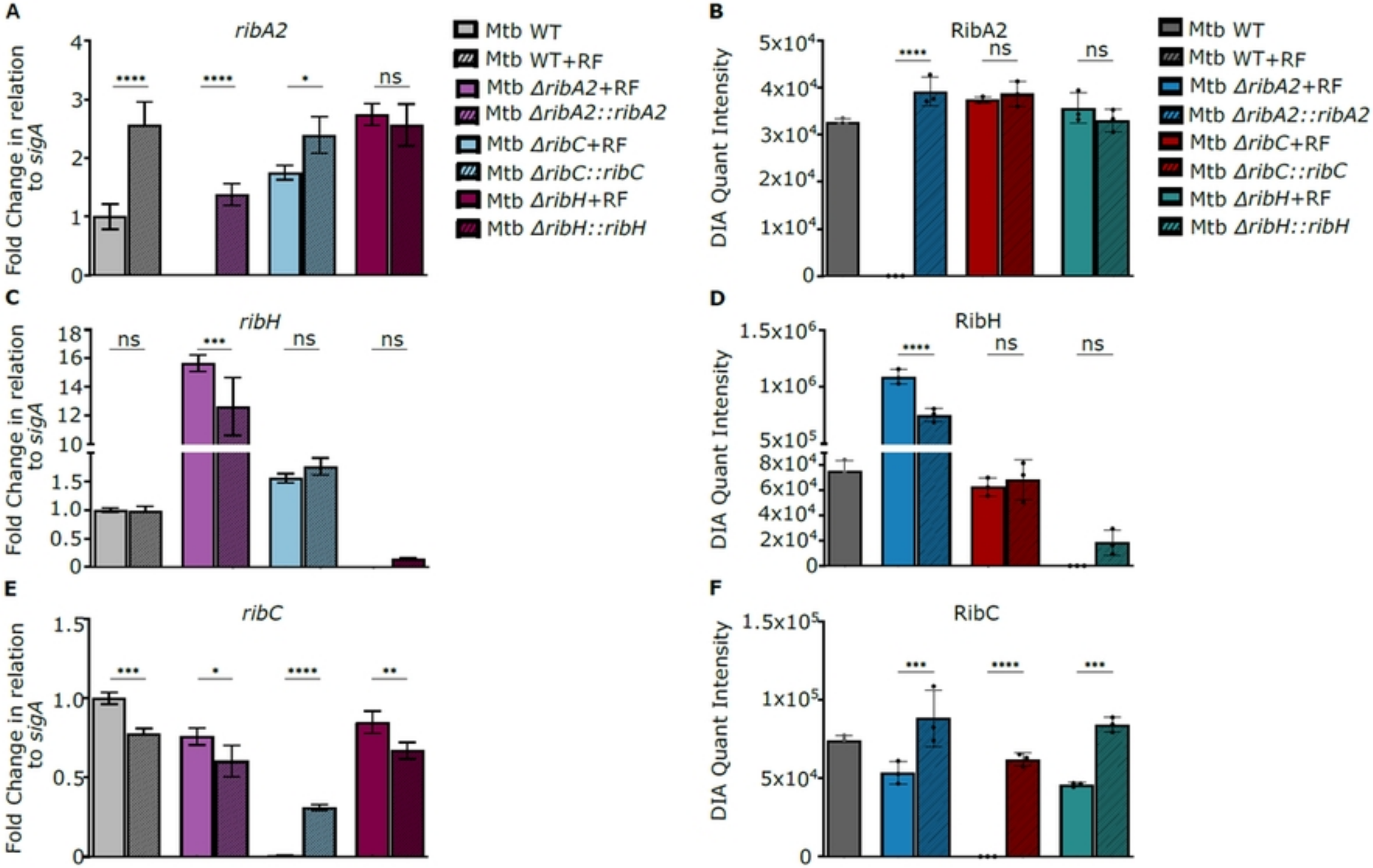
A
ribA2
Fold Change in relation to sigA
4
3
2
1
0
****
****
*
ns
Mtb WT
Mtb WT+RF
Mtb ΔribA2+RF
Mtb ΔribA2::ribA2
Mtb ΔribC+RF
Mtb ΔribC::ribC
Mtb ΔribH+RF
Mtb ΔribH::ribH
B
RibA2
DIA Quant Intensity
5x10⁴
4x10⁴
3x10⁴
2x10⁴
1x10⁴
0
****
ns
ns
C
ribH
Fold Change in relation to sigA
18
16
14
12
10
1.5
1.0
0.5
0
ns
***
ns
ns
D
RibH
DIA Quant Intensity
1.5x10⁶
1x10⁶
5x10⁵
8x10⁴
6x10⁴
4x10⁴
2x10⁴
0
****
ns
ns
E
ribC
Fold Change in relation to sigA
1.5
1.0
0.5
0
***
*
****
**
F
RibC
DIA Quant Intensity
1.5x10⁵
1x10⁵
5x10⁴
0
***
****
***

Figure 4

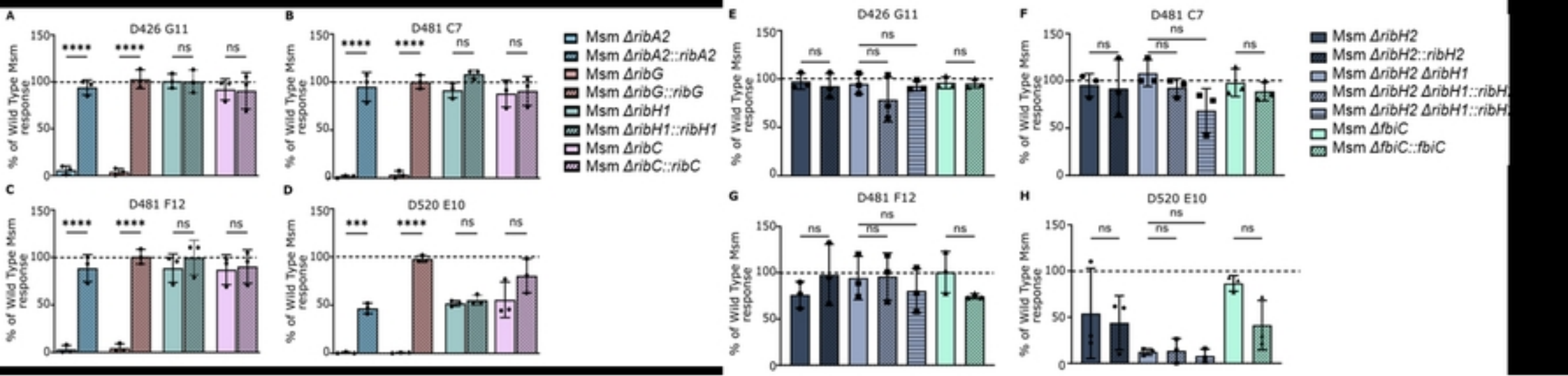
A
D426 G11
B
D481 C7
C
D481 F12
D
D520 E10
E
D426 G11
F
D481 C7
G
D481 F12
H
D520 E10
% of Wild Type Msm response
Msm ΔribA2
Msm ΔribA2::ribA2
Msm ΔribG
Msm ΔribG::ribG
Msm ΔribH1
Msm ΔribH1::ribH1
Msm ΔribC
Msm ΔribC::ribC
Msm ΔribH2
Msm ΔribH2::ribH2
Msm ΔribH2 ΔribH1
Msm ΔribH2 ΔribH1::ribH
Msm ΔribH2 ΔribH1::ribH
Msm ΔfbiC
Msm ΔfbiC::fbiC

Figure 5

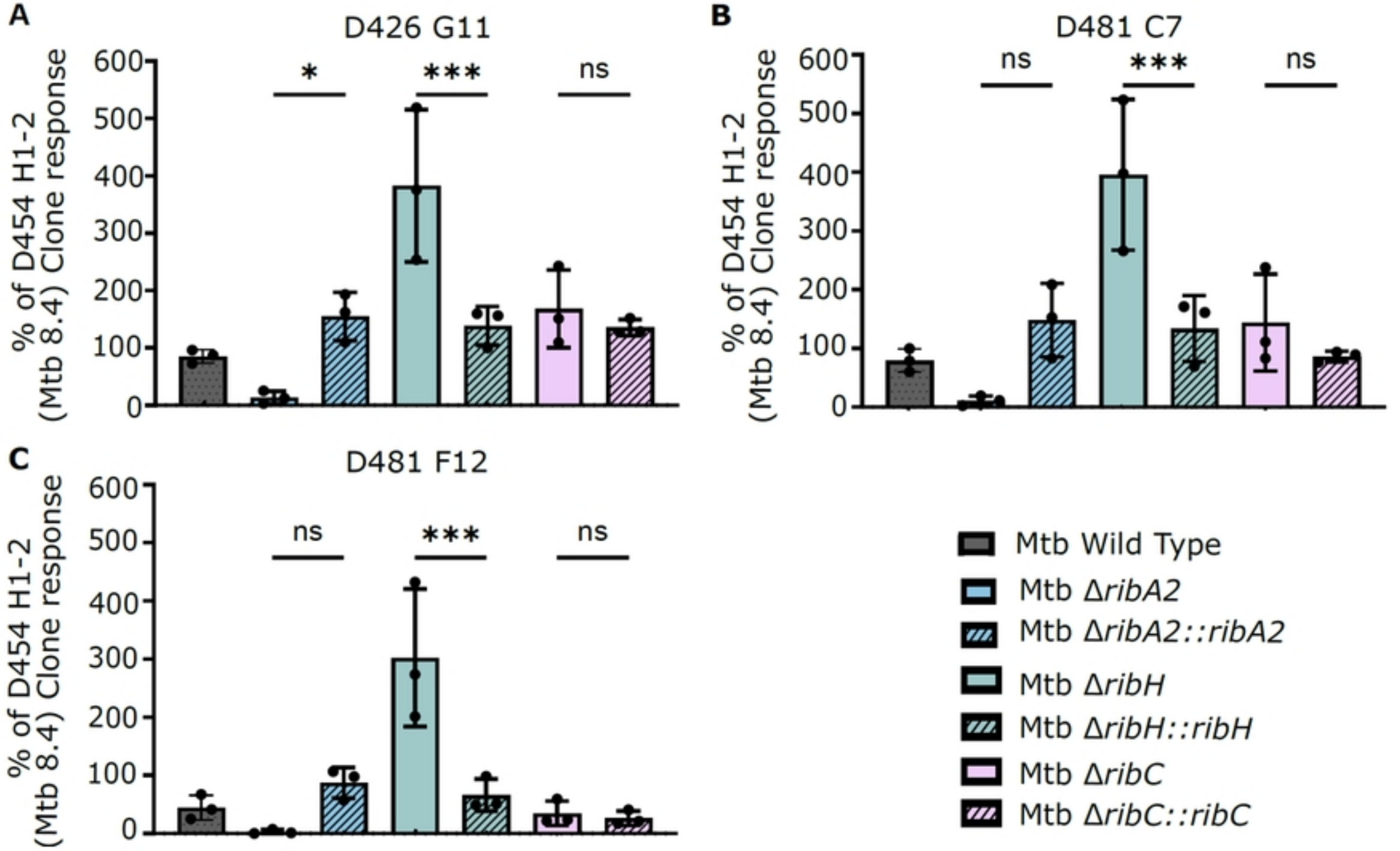
A
D426 G11
% of D454 H1-2 (Mtb 8.4) Clone response
600
500
400
300
200
100
0
*
***
ns
B
D481 C7
% of D454 H1-2 (Mtb 8.4) Clone response
ns
***
ns
C
D481 F12
% of D454 H1-2 (Mtb 8.4) Clone response
ns
***
ns
Mtb Wild Type
Mtb ΔribA2
Mtb ΔribA2::ribA2
Mtb ΔribH
Mtb ΔribH::ribH
Mtb ΔribC
Mtb ΔribC::ribC

Figure 6

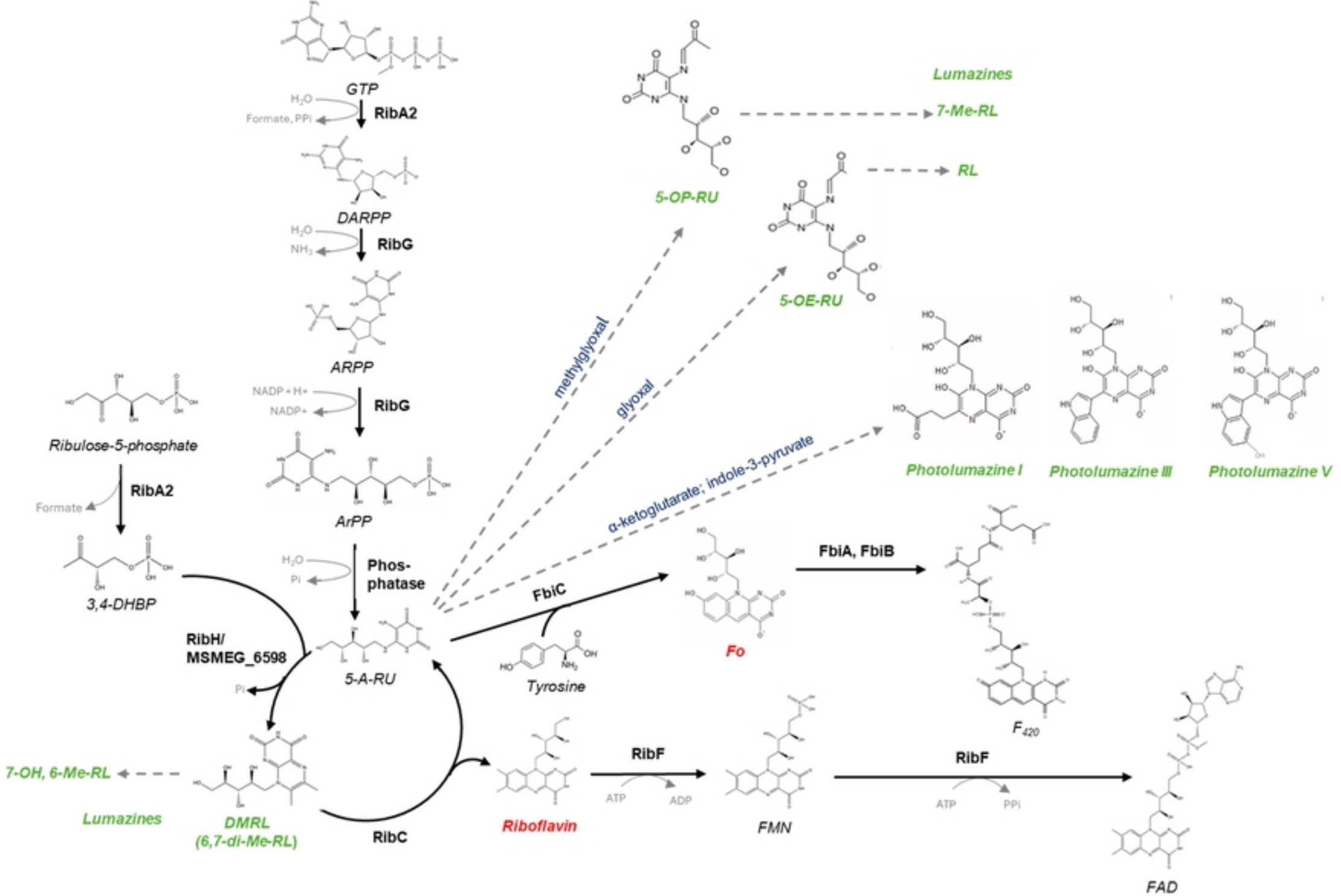
GTP
RibA2
Formate, PPi
DARPP
RibG
ARPP
RibG
NADP + H+
NADP+
ArPP
Phos-
phatase
Pi
Ribulose-5-phosphate
RibA2
Formate
3,4-DHBP
RibH/
MSMEG_6598
Pi
5-A-RU
7-OH, 6-Me-RL
Lumazines
DMRL
(6,7-di-Me-RL)
RibC
methylglyoxal
glyoxal
α-ketoglutarate; indole-3-pyruvate
5-OP-RU
5-OE-RU
Lumazines
7-Me-RL
RL
Photolumazine I
Photolumazine III
Photolumazine V
FbiC
Tyrosine
Fo
FbiA, FbiB
F420
Riboflavin
RibF
ATP
ADP
FMN
RibF
ATP
PPi
FAD

Figure 7